STRUCTURAL CHEMISTRY

ISSN: 2053-2296
journals.iucr.org/c

A polymeric silver thiosaccarinate complex with a two-dimensional triply entangled mesh and argentophilic interactions

Mariana Dennehy, Fermín Delgado, Eleonora Freire, Emilia Halac and Ricardo Baggio

Acta Cryst. (2016). C**72**, 572–577

Acta Cryst C STRUCTURAL CHEMISTRY
ISSN 2053-2296

A polymeric silver thiosaccarinate complex with a two-dimensional triply entangled mesh and argentophilic interactions

Mariana Dennehy,[a] Fermín Delgado,[a] Eleonora Freire,[b,c]*‡ Emilia Halac[b,c] and Ricardo Baggio[b]

[a]Departamento de Química (INQUISUR), Universidad Nacional del Sur, Bahía Blanca, Argentina, [b]Gerencia de Investigación y Aplicaciones, Centro Atómico Constituyentes, Comisión Nacional de Energía Atómica, Buenos Aires, Argentina, and [c]Escuela de Ciencia y Tecnología, Universidad Nacional General San Martín, Buenos Aires, Argentina. *Correspondence e-mail: freire@tandar.cnea.gov.ar

Received 13 May 2016
Accepted 14 June 2016

Edited by P. Fanwick, Purdue University, USA

‡ Member of Consejo Nacional de Investigaciones Científicas y Técnicas, Conicet.

Keywords: two-dimensional silver(I) coordination polymer; 2D–2D interpenetration; thiosaccharinate; argentophilic interaction; crystal structure; topological analysis; Raman; twinning; entangled mesh; vibrational spectroscopy.

CCDC reference: 1485531

Supporting information: this article has supporting information at journals.iucr.org/c

Silver(I) complexes with sulfur-donor ligands have a broad range of pharmacological applications. One of the most important factors for tuning the biological activity is the type of donor atom and the ease of ligand replacement. Silver thiosaccharinates display a wide range of structures from mono- to polynuclear complexes. We report the synthesis, crystal structure and vibrational spectroscopic analysis of a two-dimensional Ag^{I}–thiosaccharinate coordination polymer, namely poly[tris(μ_2-4,4′-bipyridine-κ^2N:N')bis(μ_3-1,1-dioxo-1,2-benzisothiazole-3-thiolato-κ^3N:S^3:S^3)bis(μ_2-1,1-dioxo-1,2-benzisothiazole-3-thiolato-κ^2S^3:S^3)tetrasilver(I)], $[Ag_2(C_7H_4NO_2S_2)_2(C_{10}H_8N_2)_{1.5}]_n$, with 4,4′-bipyridine acting as a spacer. A relevant feature of the structure is the presence of an unusually short Ag···Ag separation of 2.8859 (10) Å, well within the range of argentophilic interactions and confirmed as such by Raman analysis of the low-frequency spectrum. From a topological point of view, the structure presents interpenetration in the form of a threefold entangled 2D→2D mesh (2D is two-dimensional).

1. Introduction

The design and preparation of silver(I) complexes with sulfur-donor ligands has attracted increasing interest in the last few years because of their broad range of applications in pharmacological activities (Aslanidis *et al.*, 2015). In this type of complex, one of the most important factors for tuning the biological activity is the type of donor atom and the ease of ligand replacement (Glisic *et al.*, 2016).

In line with this interest, during the past decade, our group has studied the synthesis of silver thiosaccharinates (tsac is the thiosaccharinate anion), resulting in a wide range of structures from mono- to polynuclear complexes. So far, with the use of nitrogenated coligands, we have been able to obtain only two polynuclear structures, namely $[Ag(tsac)(o\text{-phen})]_n$ and $[Ag(tsac)(4\text{-MeOpy})]_n$ (o-phen is *ortho*-phenantroline and 4-MeOpy is 4-methoxypyridine), both of which have long Ag···S interactions (Dennehy *et al.*, 2008, 2010). In the search for a polymeric silver thiosaccharinate structure, we choose the 4,4′-bipyridine (4,4′-bpy) coligand because of its potential as a bridging ligand. We first tried to prepare a ternary 4,4′-bpy thiosaccharinate using PPh_3 in the mother solution in order to increase the solubility of $Ag_6(tsac)_6$ in CH_3CN. Surprisingly, we obtained $[Ag_4(tsac)_4(PPh_3)_4]$ (Dennehy *et al.*, 2007), with the 4,4′-bpy ligand being absent from the complex. Finally, the use of dimethyl sulfoxide (DMSO), acting as a coordinating

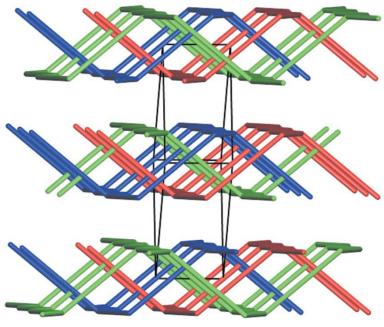

solvent, facilitated the binding of 4,4′-bpy. Thus, we report herein the synthesis and crystal structure of a thiosaccharinate coordination polymer with 4,4′-bpy, namely $[Ag_2(tsac)_2(4,4'\text{-bpy})_{1.5}]_n$, (I). This is an interesting structure both from a strictly chemical point of view (it presents an Ag···Ag separation well within the range of argentophilic interactions) and from a crystallographic point of view (the packing is based on a threefold entangled 2D→2D mesh).

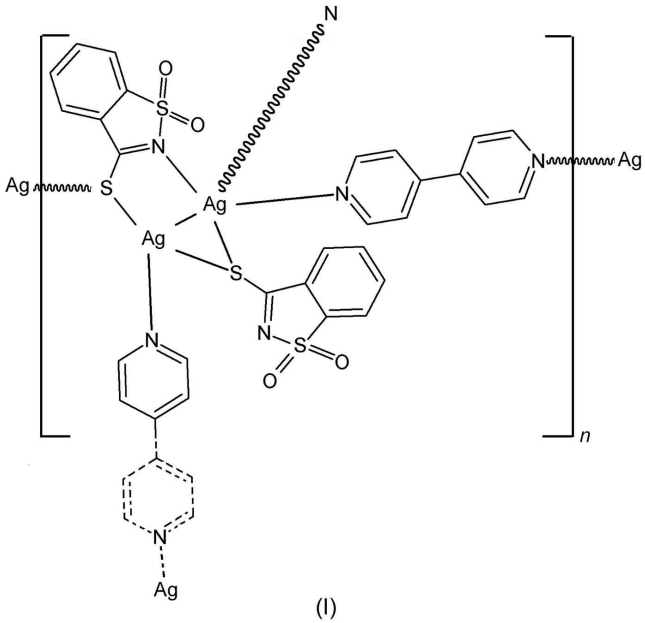

(I)

Scheme 1

2. Experimental

2.1. Synthesis and crystallization

The title complex was synthesized by the addition of a solution of $AgNO_3$ (24 mg) in MeCN (6 ml) to an MeCN solution (6 ml) of thiosaccharine (30 mg) kept under mechanical stirring at room temperature. The resulting yellow solid was filtered off (yield 89%) and washed with diethyl ether. Solid $Ag_6(tsac)_6$ (12 mg) was dissolved in dimethyl sulfoxide (2 ml). 4,4′-Bipyridine (4,4′-bpy, 12 mg) was added to the obtained yellow solution. Slow diffusion of CH_2Cl_2 into this solution yielded yellow plate-shaped crystals of $[Ag_2(tsac)_2(4,4'\text{-bpy})_{1.5}]_n$, (I), suitable for X-ray diffraction studies. The same complex was obtained when the synthesis was carried out in dimethylformamide (DMFA).

Analytical composition calculated for $C_{29}H_{20}Ag_2N_5O_4S_4$: C 41.15, H 2.38, N 8.27%; found: C 40.56, H 2.16, N 7.83%.

2.2. Refinement

Crystal data, data collection and structure refinement details are summarized in Table 1. The crystal measured was a two-component nonmerohedral twin, each individual data set having the following characteristics: number of reflections: 39893/40773; R(sym): 0.105 [4647]/0.157 [4748], mean (I/σ): 11.21/8.17, for the 1st/2nd individual, respectively. The initial model was obtained in a straightforward manner with data from one component and further refined with a combined set through the HKLF 5 instruction in *SHELXL2014* (Sheldrick, 2015). Some similarity restraints were used to facilitate refinement and convergence to a suitable model.

H atoms were found in a difference map, were further idealized and were finally refined as riding, with aromatic C—H = 0.93 Å and $U_{iso}(H) = 1.2U_{eq}(C)$.

Table 1
Experimental details.

Crystal data	
Chemical formula	$[Ag_2(C_7H_4NO_2S_2)_2(C_{10}H_8N_2)_{1.5}]$
M_r	846.48
Crystal system, space group	Monoclinic, $P2_1/n$
Temperature (K)	294
a, b, c (Å)	15.3542 (4), 7.9565 (2), 24.8986 (6)
β (°)	98.477 (2)
V (Å^3)	3008.52 (13)
Z	4
Radiation type	Mo $K\alpha$
μ (mm^{-1})	1.63
Crystal size (mm)	0.24 × 0.18 × 0.10
Data collection	
Diffractometer	Oxford Diffraction Gemini CCD S Ultra
Absorption correction	Multi-scan (*CrysAlis PRO*; Oxford Diffraction, 2009)
No. of measured, independent and observed $[I > 2\sigma(I)]$ reflections	8912, 8912, 7674
$(\sin\theta/\lambda)_{max}$ (Å^{-1})	0.688
Refinement	
$R[F^2 > 2\sigma(F^2)]$, $wR(F^2)$, S	0.066, 0.171, 1.17
No. of reflections	8912
No. of parameters	398
No. of restraints	403
H-atom treatment	H-atom parameters constrained
$\Delta\rho_{max}$, $\Delta\rho_{min}$ (e Å^{-3})	1.05, −1.29

Computer programs: *CrysAlis PRO* (Oxford Diffraction, 2009), *SHELXS97* (Sheldrick, 2008), *SHELXTL* (Sheldrick, 2008), *ToposPro* (Blatov *et al.*, 2014), *SHELXL2014* (Sheldrick, 2015) and *PLATON* (Spek, 2009).

2.3. Spectroscopic analysis

IR spectra were obtained on an FT–IR–NIR Thermo Scientific Nicolet iS50 (KBr dispersion, ν, cm^{-1}): 1465 (*m*), 1411 (*m*), 1388 (*m*), 1313 (*m*), 1231 (*m*), 1164 (*s*), 1156 (*w*), 1003 (*m*), 991 (*m*), 950 (*w*), 811 (*m*), 797 (*m*), 778 (*w*), 623 (*w*), 585 (*m*), 554 (*m*), 537 (*m*), 436 (*m*).

The Raman spectra, in turn, were recorded with a LabRAM HR Horiba Jobin Yvon Raman system equipped with two monochromator gratings and a charge-coupled device detector. A 1800 g mm^{-1} grating and a 50 µm hole resulted in a spectral resolution of 1.5 cm^{-1}. The spectrograph was coupled to an imaging microscope with 10×, 50× and 100× magnifications. The He–Ne laser line at 632.8 nm was used as the excitation source. Each spectrum was averaged over eight scans, with a collection time of 120 s for each scan. The Raman spectra were acquired on powder samples at room temperature and at 80 K. For the low-temperature spectra, the sample was placed on a Linkam Examina THMS600 Temperature-Controlled Stage. Measurements were carried out using a backscattering geometry, with 10× magnification.

3. Results and discussion

3.1. Structural and topological analysis

The asymmetric unit of (I) (Fig. 1) consists of two Ag^{I} cations, two anionic tsac ligands, denoted tsac(*A*) and tsac(*B*), and one and a half 4,4′-bpy molecules, with 4,4′-bpy(*C*) lying in a general position and 4,4′-bpy(*D*) halved by an inversion centre.

The tsac ligands are featureless, not departing from their expected geometry. The 4,4′-bpy ligands, in contrast, are quite dissimilar. While centrosymmetric 4,4′-bpy(*D*) is perfectly planar, 4,4′-bpy(*C*) is highly deformed, through a combination of bending [as measured by the deviation from 90° of the angles which the normals to the pyridyl planes subtend with the central C3*C*—C8*C* bond, *i.e.* 5.4 (4) and 6.9 (5)°, respectively, where a value of 0° indicates no bending of the pyridyl groups] and rotation, to end up with an interplanar angle between the pyridine rings of 39.6 (4)°.

Regarding coordination, the tsac ligands bind both Ag^{I} cations, *i.e.* tsac(*A*) by chelation through an N1*A*—Ag1—S1*A* bite and tsac(*B*) *via* the bridging S2*B* atom. As a result of this two-sided bridging, the Ag^{I} atoms end up at a 'ligand-assisted' argentophilic interaction distance of 2.8859 (10) Å (Kristiansson, 2001; Castiñeiras *et al.*, 2006; Schmidbaur & Schier, 2015), a point which will be discussed below. The 4,4′-bpy ligands, in turn, link one Ag^{I} atom at each end.

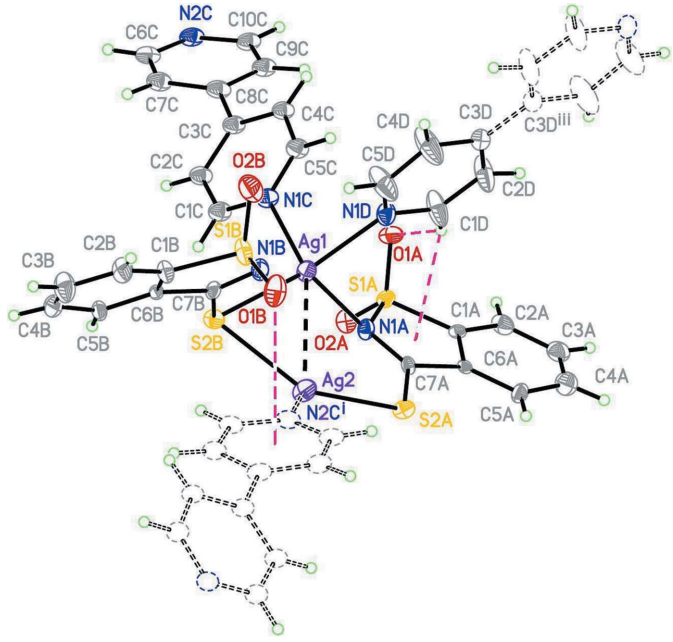

Figure 1
Displacement ellipsoid plot (40% probability level) of the asymmetric unit in (I). The symmetry-related part completing the coordination sphere is indicated with double broken lines and intramolecular hydrogen bonds are indicated with simple broken lines. [Symmetry codes: (i) $x-\frac{1}{2}, -y+\frac{1}{2}, z-\frac{1}{2}$; (iii) $-x+2, -y+2, -z$.]

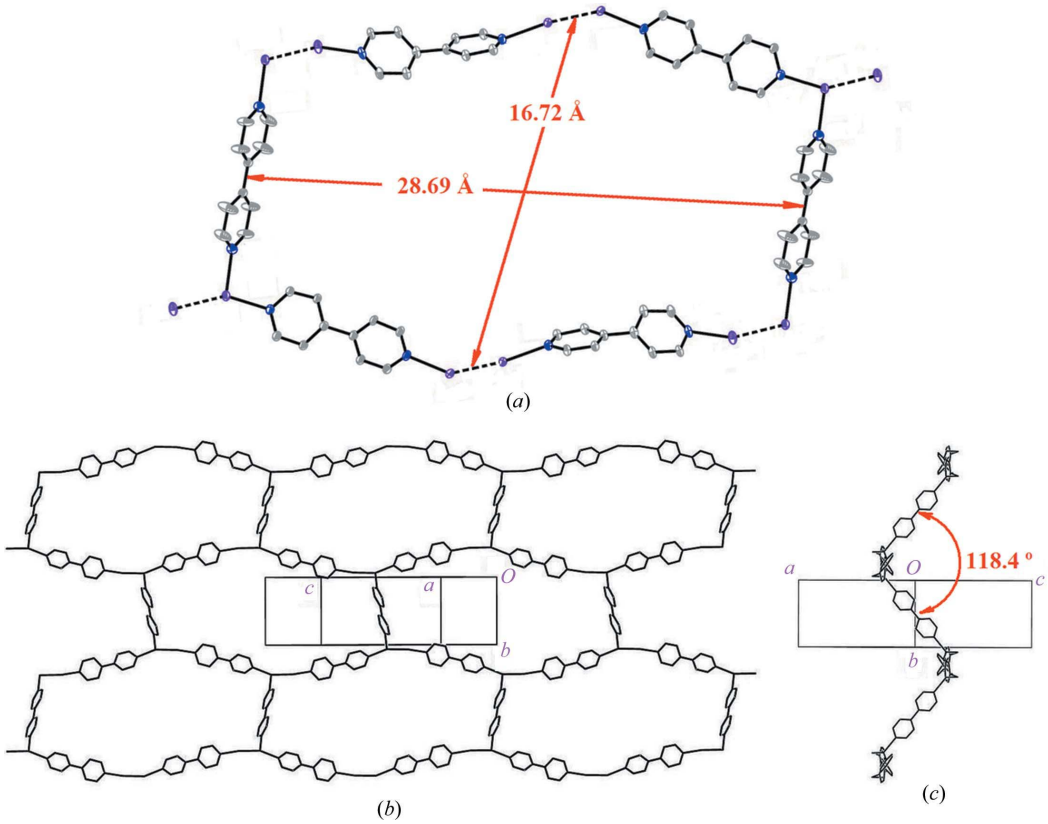

Figure 2
(*a*) A simplified view of the 'open' mesh in (I) (tsac units are not shown for clarity). (*b*) A projection of the (001) plane, showing an individual two-dimensional structure, *i.e.* the elemental unit of the entangled net. (*c*) The same motif as shown in part (*b*) but rotated by 90° ([101] projection), showing the zigzag character of the corrugated net.

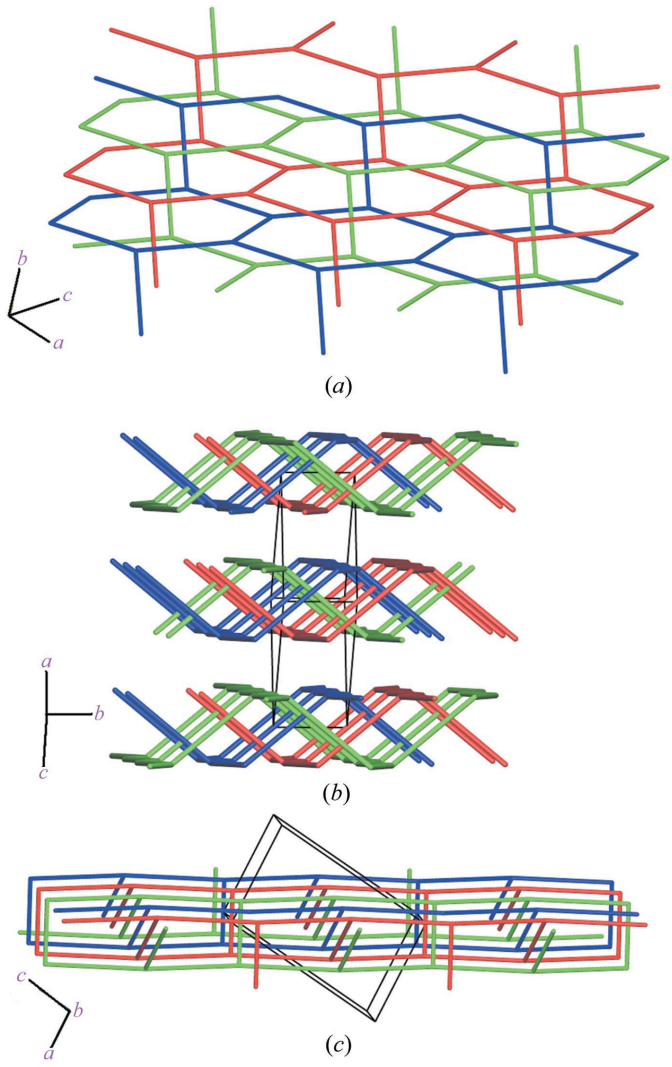

Figure 3
(*a*) A detailed view showing the way in which the three (differently coloured) nets interpenetrate to form a broad ($\bar{1}01$) slab. (*b*)/(*c*) Lateral views of the resulting slabs. The figure was prepared with *ToposPro* (Blatov *et al.*, 2014).

The resulting coordination of each Ag^{I} cation can be seen in Fig. 1. Ag1 is four-coordinated in an AgN_3S distorted tetrahedral environment, while Ag2 is three-coordinated in a quasi-planar $AgNS_2$ environment, 0.259 (2) Å away from the least-squares plane defined by the ligands. Table 2 reports the coordination distances and angles.

The role of the spacers fulfilled by 4,4′-bpy(*C*) and 4,4′-bpy(*D*) results in a (6,3) honeycomb structure, with a very open mesh (~26.89 Å long × ~16.72 Å wide), schematically depicted in Fig. 2(*a*). The resulting sheets (Fig. 2*b*) are severely corrugated (Fig. 2*c*), with a zigzag angle of ~118.4 (2)°. It is well known that both facts (*viz.* the existence of a mesh with a large window size, in conjunction with corrugation) is a favourable situation for interpenetration (Batten, 2001), that is, the formation of entangled nets which cannot be separated without the breakage of at least one bond.

This is in fact the case here, where interpenetration of further networks shifted by a [010] vector takes place, to end

Table 2
Selected geometric parameters (Å, °).

Ag1—N1*D*	2.312 (8)	Ag2—N2*C*^{i}	2.349 (8)
Ag1—N1*C*	2.373 (7)	Ag2—S2*A*	2.448 (2)
Ag1—S2*B*	2.492 (2)	Ag2—S2*B*	2.566 (2)
Ag1—N1*A*	2.502 (8)		
Ag2···S2*A*^{ii}	3.046 (2)		
N1*D*—Ag1—N1*C*	97.0 (3)	S2*B*—Ag1—N1*A*	117.91 (18)
N1*D*—Ag1—S2*B*	137.1 (2)	N2*C*^{i}—Ag2—S2*A*	118.3 (2)
N1*C*—Ag1—S2*B*	103.3 (2)	N2*C*^{i}—Ag2—S2*B*	97.0 (2)
N1*D*—Ag1—N1*A*	96.3 (3)	S2*A*—Ag2—S2*B*	141.04 (8)
N1*C*—Ag1—N1*A*	96.7 (2)		

Symmetry codes: (i) $x-\frac{1}{2}, -y+\frac{1}{2}, z-\frac{1}{2}$; (ii) $-x+1, -y+1, -z$.

up with the 2D→2D entanglement (2D is two-dimensional) of three single sheets, shown in Fig. 3(*a*), with the final result of broad slabs parallel to ($\bar{1}01$). This kind of entanglement is not rare since it has been reported 40 times since 1995 (see Carlucci *et al.*, 2014). There are, however, only three examples in the literature of threefold interpenetrated (6,3) nets with silver, *viz. catena*-[hexakis(μ_2-cyano-κ^2C:*N*)bis(ethylenediamine-κ^2N,N')nickeltetrasilver] (Duriska *et al.*, 2006), *catena*-[bis(glutarato-κO)pentakis(μ_2-3,3′,5,5′-tetramethyl-1*H*,1′*H*-4,4′-bipyrazole)tetrasilver] and *catena*-[bis(adipato-κO)pentakis(μ_2-3,3′,5,5′-tetramethyl-1*H*,1′*H*-4,4′-bipyrazole)tetrasilver] (Han *et al.*, 2014).

Regarding weak interactions, in this scenario of interpenetration we found it useful to classify them by the structural effect which the interactions have on the coherence of the structure. Thus, we found contacts internal to one single sheet (hereinafter Type I), those connecting entangled nets in the same slab (Type II) and those relating different slabs (Type III). Tables 3 and 4 present the most relevant of these interactions, characterized by their 'Type', as defined above. In particular, Type I contacts are shown in Fig. 1. In all cases, these interactions stabilizing the 'crisscross' structure are weak

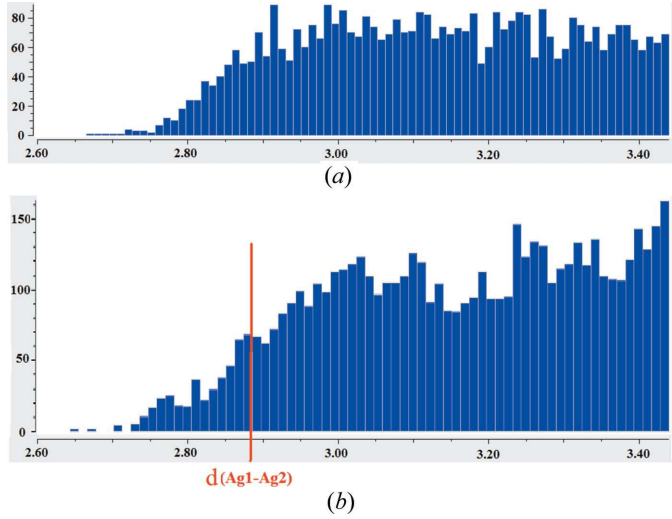

Figure 4
The distribution of Ag···Ag short contacts (CSD; Groom & Allen, 2014). (*a*) The unsupported interactions and (*b*) the supported interactions. The Ag···Ag distance in (I) is highlighted.

Table 3
D—$X\cdots A$ interactions in (I) (Å, °).

*Cg*1 is the centroid of the S1*A*/N1*A*/C7*A*/C6*A*/C1*A* ring, *Cg*2 is the centroid of the N1*D*/C1*D*–C5*D* ring, *Cg*3 is the centroid of the N2*C*/C6*C*–C10*C* ring, *Cg*4 is the centroid of the C1*A*–C6*A* ring and *Cg*5 is the centroid of the C1*B*–C6*B* ring.

D—$X\cdots A$	D—X	$X\cdots A$	$D\cdots A$	D—$X\cdots A$	Type
C1*D*—H1*D*$\cdots$O1*A*	0.93	2.59	3.345 (13)	139	I
C1*D*—H1*D*$\cdots$*Cg*1	0.93	2.93	3.759 (14)	150	I
S1*B*—O1*B*$\cdots$*Cg*3^{i}	1.427 (8)	3.564 (10)	4.332 (5)	113.3 (4)	I
C5*C*—H5*C*$\cdots$O2*B*^{iv}	0.93	2.48	3.189 (13)	134	II
C1*C*—H1*C*$\cdots$*Cg*4^{v}	0.93	2.89	3.704 (10)	147	II
C2*A*—H2*A*$\cdots$O2*A*^{vi}	0.93	2.56	3.383 (11)	147	III
S1*A*—O2*A*$\cdots$*Cg*3^{vi}	1.434 (6)	3.469 (7)	4.065 (4)	104.2 (3)	III

Symmetry codes: (i) $x-\frac{1}{2}, -y+\frac{1}{2}, z-\frac{1}{2}$; (iv) $-x+2, -y+1, -z$; (v) $x, y-1, z$; (vi) $-x+\frac{3}{2}, y+\frac{1}{2}, -z+\frac{1}{2}$; (vii) $-x+\frac{3}{2}, y-\frac{1}{2}, -z+\frac{1}{2}$.

and of a large variety (C—H$\cdots$O, C—H$\cdots\pi$, S—O$\cdots\pi$ and π–π, and even a short Ag$\cdots$S contact, which is included in Table 2) with no particular dominance of any of them.

3.2. Argentophilic interactions

An argentophilic interaction is a silver–silver metal bond suspected to be present in any molecular or crystal structure. Low-coordinate Ag^{I} cations with a d^{10} electronic configuration appear within Ag$\cdots$Ag distances shorter than 3.44 Å, twice the van der Waals radius of Ag^{I} (Bondi, 1964).

These contacts can be further classified either as 'supported' or 'unsupported', depending on the presence or absence of any ligand bridging the Ag^{I} cations in question.

Even if the statistical distribution of these two types of contacts are rather similar [Figs. 4*a* and 4*b*; data taken from the Cambridge Structural Database (CSD, Version 5.36, with one update; Groom & Allen, 2014)], there are intrinsic differences in their assessment. In the unsupported case, the significance of the Ag$\cdots$Ag contact is rather easy to evaluate since it often represents the closest approach between independent molecular units, without the existence of anything forcing the approach. In the case of bridged or 'ligand-supported' contacts, instead, the significance of any presumed argentophilic interactions evaluated only on the bases of intermetallic distances alone is much less reliable due to the potential effect that the ligand bridges may have in the Ag$\cdots$Ag shortening.

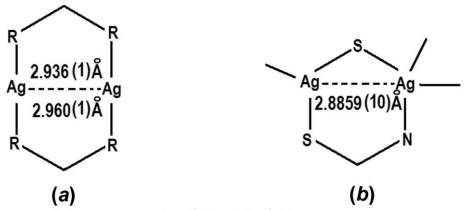

Scheme 2

A way to circumvent this drawback is to resort to vibrational spectroscopic techniques, like IR and Raman. Unfortunately, multi-ligand compounds give rise to complex IR and Raman spectra which are difficult to interpret, with Ag$\cdots$Ag

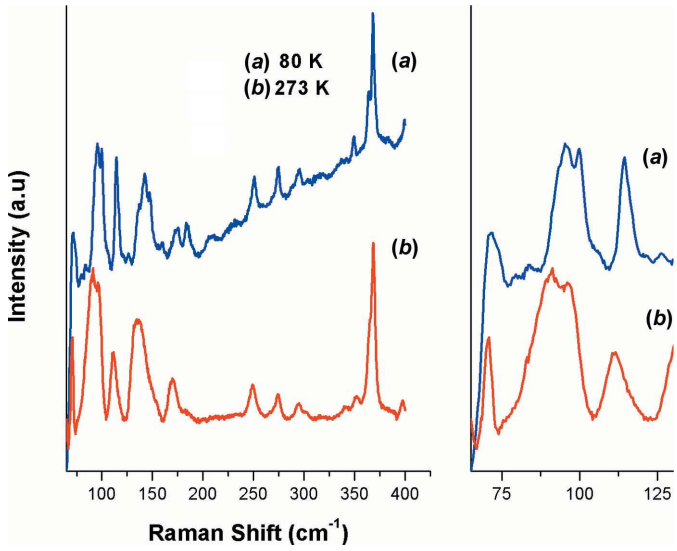

Figure 5
The Raman spectra of (I) recorded at room temperature and at 80 K. Left: frequency range up to 400 cm^{-1}. Right: an expanded view of the low-frequency region. (Note that the narrow band at about 70 cm^{-1} is an artifact of the laser notch filter.)

vibrations occurring at rather low frequencies and sometimes overlapping lattice bands. The result is that there are few studies which have so far provided solid evidence for Ag$\cdots$Ag bonding. There are, however, a handful of cases in the literature reporting successful Raman studies of argentophilic interactions, both in unsupported (*e.g.* Omary *et al.*, 1998) and supported cases. One example is the di-supported (two bridges) argentophilic interaction reported in Perreault *et al.* (1992) for the cyclic dications shown in part (*a*) of Scheme 2. Similar to the present case, the reported Ag$\cdots$Ag distances of 2.936 (1) and 2.960 (1) Å for two independent molecules were at the time interpreted as a signal of significant bonding. There have been some more quantitative approaches to the subject, for example, those by Harvey and co-workers (Perreault *et al.*, 1993; Harvey, 1996), who observed a linear correlation between the Ag_2 bond distance, $r(Ag_2)$, and the associated Force Constant, $F(Ag_2)$, for nine binuclear Ag_2 compounds, *viz.* $r(Ag_2) = -0.284\ln F(Ag_2) + 2.53$.

Looking for further evidence in order to reinforce our metric arguments in support of an argentophilic interaction in (I), a Raman study of its double-bridged system [see part (*b*) of Scheme 2] was attempted.

Table 4
π–π contacts for (I).

For ring-centroid (*Cg*) definitions, see Table 3. ccd is the centre-to-centre distance (distance between ring centroids), da is the dihedral angle and ipd is the (mean) interplanar distance (distance from one plane to the neighbouring centroid). For further details, see Janiak (2000).

Group1$\cdots$Group2	ccd (Å)	da (°)	mipd (Å)	Type
*Cg*5$\cdots$*Cg*2^{v}	4.068 (7)	19.8 (6)	3.5 (2)	II
*Cg*3$\cdots$*Cg*4^{vii}	4.061 (6)	16.4 (4)	3.3 (3)	III

Symmetry codes: (v) $x, y-1, z$; (vii) $-x+\frac{3}{2}, y-\frac{1}{2}, -z+\frac{1}{2}$.

Fig. 5 shows the Raman spectra at room temperature and at 80 K. It can be seen that a strong peak at 91 cm^{-1} (with a shoulder at 96 cm^{-1}) at room temperature is resolved into two bands at 95 and 100 cm^{-1} at 80 K.

For the Ag1$\cdots$ Ag2 distance in (I) [2.8859 (10) Å at 294 K], Harvey's curve predicts a force constant $F(Ag_2)$ = 0.285598 mdyn A^{-1} and an Ag–Ag stretching frequency of 94.89 cm^{-1}. The observed band in (I) is in excellent agreement with the expected Ag_2 stretching frequencies.

The remaining bands at 249 and 274 cm^{-1} could be assigned to Ag—S stretching modes, as described for similar compounds (Bensebaa *et al.*, 1999; Martina *et al.*, 2012) and the strong bands at 364–368 cm^{-1} to Ag—N stretching. The bands at 133 and 169 cm^{-1} could be related to Ag—N ring modes. Two weak bands observed in the low-temperature spectrum at 79 and 84 cm^{-1} are slightly distinguished as a shoulder at room temperature. Bands of this type, around 80 cm^{-1}, have been assigned to Ag–Ag modes in other argentophilic compounds (Omary *et al.*, 1998; Che *et al.*, 2000). However, a more detailed assignment in our spectra would require a complete frequency calculation, something which is far beyond the original scope of the present work; our Raman study was aimed at the confirmation of the argentophilic character of the Ag$\cdots$Ag interaction in (I), a fully accomplished objective.

Acknowledgements

The authors acknowledge NPCyT (project No. PME 2006-01113) for the purchase of the Oxford Gemini CCD diffractometer. MD and FD thank SGCyT–UNS for financial support under Project M24/Q043. The authors are also indebted to Professor Davide Proserpio for his help in the proper use of *ToposPro*.

References

Aslanidis, P., Hatzidimitriou, A. G., Andreadou, E. G., Pantazaki, A. A. & Voulgarakis, N. (2015). *Mater. Sci. Eng. C*, **50**, 187–193.
Batten, S. R. (2001). *CrystEngComm*, **18**, 1–7.
Bensebaa, F., Zhou, Y., Brolo, A. G., Irish, D. E., Deslandes, Y., Kruus, E. & Ellis, T. H. (1999). *Spectrochim. Acta Part A*, **55**, 1229–1236.
Blatov, V. A., Shevchenko, A. P. & Proserpio, D. M. (2014). *Cryst. Growth Des.* **14**, 3576–3586.
Bondi, A. (1964). *J. Phys. Chem.* **68**, 441–451.
Carlucci, L., Ciani, C., Proserpio, D. M., Mitina, T. G. & Blatov, V. A. (2014). *Chem. Rev.* **114**, 7557–7580.
Castiñeiras, A., García-Santos, I., Dehnen, S. & Sevillano, P. (2006). *Polyhedron*, **25**, 3653–3660.
Che, C.-M., Tse, M.-C., Chan, M. C. W., Cheung, K.-K., Phillips, D. L. & Leung, K.-H. (2000). *J. Am. Chem. Soc.* **122**, 2464–2468.
Dennehy, M., Ferullo, R. M., Quinzani, O. V., Mandolesi, S. D., Castellani, N. & Jennings, M. (2008). *Polyhedron*, **27**, 2243–2250.
Dennehy, M., Mandolesi, S. D., QuinzaniaO, V. & Jenning, M. (2007). *Z. Anorg. Allg. Chem.* **633**, 2746–2752.
Dennehy, M., Quinzani, O. V., Granados, A. & Burrow, R. A. (2010). *Polyhedron*, **29**, 1344–1352.
Duriska, M. B., Batten, S. R. & Price, D. J. (2006). *Aust. J. Chem.* **59**, 26–29.
Glisic, B. D., Senerovic, L., Comba, P., Wadepohl, H., Veselinovic, A., Milivojevic, D. L., Djuran, M. I. & Nikodinovic-Runic, J. (2016). *J. Inorg. Biochem.* **155**, 115–128.
Groom, C. R. & Allen, F. H. (2014). *Angew. Chem. Int. Ed.* **53**, 662–671.
Han, L.-L., Zhang, X.-Y., Chen, J.-S., Li, Z.-H., Sun, D.-F., Wang, X.-P. & Sun, D. (2014). *Cryst. Growth Des.* **14**, 2230–2239.
Harvey, P. D. (1996). *Coord. Chem. Rev.* **153**, 175–198.
Janiak, C. (2000). *J. Chem. Soc. Dalton Trans.* pp. 3885–3898.
Kristiansson, O. (2001). *Inorg. Chem.* **40**, 5058–5059.
Martina, I., Wiesinger, R., Jembrih-Simbürger, D. & Schreiner, M. (2012). *e-Preserv. Sci.* **9**, 1–8.
Omary, M. A., Webb, T. R., Assefa, Z., Shankle, G. E. & Patterson, H. H. (1998). *Inorg. Chem.* **37**, 1380–1386.
Oxford Diffraction (2009). *CrysAlis PRO*. Oxford Diffraction Ltd, Abingdon, Oxfordshire, England.
Perreault, D., Drouin, M., Michel, A. & Harvey, P. D. (1993). *Inorg. Chem.* **32**, 1903–1912.
Perreault, D., Drouin, M., Michel, A., Viskowski, V. M., Schaefer, W. P. & Harvey, P. D. (1992). *Inorg. Chem.* **31**, 695–702.
Schmidbaur, H. & Schier, A. (2015). *Angew. Chem. Int. Ed.* **54**, 746–784.
Sheldrick, G. M. (2008). *Acta Cryst.* A**64**, 112–122.
Sheldrick, G. M. (2015). *Acta Cryst.* C**71**, 3–8.
Spek, A. L. (2009). *Acta Cryst.* D**65**, 148–155.

supporting information

Acta Cryst. (2016). C**72**, 572-577 [doi:10.1107/S2053229616009645]

A polymeric silver thiosaccarinate complex with a two-dimensional triply entangled mesh and argentophilic interactions

Mariana Dennehy, Fermín Delgado, Eleonora Freire, Emilia Halac and Ricardo Baggio

Computing details

Data collection: *CrysAlis PRO* (Oxford Diffraction, 2009); cell refinement: *CrysAlis PRO* (Oxford Diffraction, 2009); data reduction: *CrysAlis PRO* (Oxford Diffraction, 2009); program(s) used to solve structure: *SHELXS97* (Sheldrick, 2008); program(s) used to refine structure: *SHELXL2014* (Sheldrick, 2015); molecular graphics: *SHELXTL* (Sheldrick, 2008) and *ToposPro* (Blatov *et al.* (2014); software used to prepare material for publication: *SHELXL2014* (Sheldrick, 2015) and *PLATON* (Spek, 2009).

Bis(μ_3-1,1-dioxo-1,2-benzisothiazole-3-thiolato-κ^3N:S^3:S^3)bis(μ_2-1,1-dioxo-1,2-benzisothiazole-3-thiolato-κ^2S^3:S^3)tetrasilver(I)]

Crystal data

$[Ag_2(C_7H_4NO_2S_2)_2(C_{10}H_8N_2)_{1.5}]$
M_r = 846.48
Monoclinic, $P2_1/n$
a = 15.3542 (4) Å
b = 7.9565 (2) Å
c = 24.8986 (6) Å
β = 98.477 (2)°
V = 3008.52 (13) Å^3
Z = 4
$F(000)$ = 1676
D_x = 1.869 Mg m^{-3}
Mo $K\alpha$ radiation, λ = 0.71073 Å
Cell parameters from 19239 reflections
θ = 3.7–28.8°
μ = 1.63 mm^{-1}
T = 294 K
Plate, pale_yellow
0.24 × 0.18 × 0.10 mm

Data collection

Oxford Diffraction Gemini CCD S Ultra diffractometer
ω scans, thick slices
Absorption correction: multi-scan (CrysAlis PRO; Oxford Diffraction, 2009)
8912 measured reflections
8912 independent reflections
7674 reflections with $I > 2\sigma(I)$
θ_{max} = 29.3°, θ_{min} = 3.6°
h = −20→21
k = −10→10
l = −33→33

Refinement

Refinement on F^2
Least-squares matrix: full
$R[F^2 > 2\sigma(F^2)]$ = 0.066
$wR(F^2)$ = 0.171
S = 1.17
8912 reflections
398 parameters
403 restraints
Hydrogen site location: inferred from neighbouring sites
H-atom parameters constrained
$w = 1/[\sigma^2(F_o^2) + (0.0545P)^2 + 36.2817P]$ where $P = (F_o^2 + 2F_c^2)/3$
$(\Delta/\sigma)_{max}$ = 0.001
$\Delta\rho_{max}$ = 1.05 e Å^{-3}
$\Delta\rho_{min}$ = −1.29 e Å^{-3}

Special details

Geometry. All esds (except the esd in the dihedral angle between two l.s. planes) are estimated using the full covariance matrix. The cell esds are taken into account individually in the estimation of esds in distances, angles and torsion angles; correlations between esds in cell parameters are only used when they are defined by crystal symmetry. An approximate (isotropic) treatment of cell esds is used for estimating esds involving l.s. planes.

Refinement. Refined as a 2-component twin

Fractional atomic coordinates and isotropic or equivalent isotropic displacement parameters (Å²)

	x	*y*	*z*	U_{iso}*/U_{eq}
Ag1	0.77241 (5)	0.43764 (9)	0.04029 (3)	0.02539 (16)
Ag2	0.60461 (5)	0.43249 (10)	−0.02934 (3)	0.03308 (19)
S1A	0.71399 (14)	0.6533 (3)	0.15914 (8)	0.0199 (4)
S2A	0.57103 (15)	0.7075 (3)	0.00667 (9)	0.0227 (4)
N1A	0.6780 (5)	0.6002 (9)	0.0956 (3)	0.0219 (8)
O1A	0.8078 (4)	0.6691 (9)	0.1679 (3)	0.0303 (14)
O2A	0.6766 (4)	0.5412 (8)	0.1947 (2)	0.0276 (13)
C1A	0.6659 (5)	0.8530 (10)	0.1558 (3)	0.0155 (12)
C2A	0.6708 (6)	0.9772 (12)	0.1946 (4)	0.0287 (16)
H2A	0.6987	0.9586	0.2298	0.034*
C3A	0.6323 (7)	1.1321 (14)	0.1792 (4)	0.0340 (17)
H3A	0.6343	1.2190	0.2044	0.041*
C4A	0.5917 (7)	1.1558 (14)	0.1271 (4)	0.0374 (19)
H4A	0.5685	1.2612	0.1172	0.045*
C5A	0.5835 (6)	1.0279 (10)	0.0878 (4)	0.0237 (15)
H5A	0.5544	1.0457	0.0528	0.028*
C6A	0.6208 (5)	0.8742 (10)	0.1037 (3)	0.0137 (12)
C7A	0.6276 (6)	0.7184 (10)	0.0710 (3)	0.0160 (12)
S1B	0.82646 (19)	0.2697 (3)	−0.14337 (11)	0.0331 (5)
S2B	0.70851 (15)	0.1810 (3)	−0.00764 (9)	0.0246 (3)
N1B	0.7919 (5)	0.3130 (9)	−0.0849 (3)	0.0267 (13)
O1B	0.7743 (6)	0.3588 (9)	−0.1864 (3)	0.0452 (17)
O2B	0.9194 (6)	0.2911 (10)	−0.1374 (4)	0.054 (2)
C1B	0.7973 (6)	0.0520 (11)	−0.1444 (4)	0.0236 (14)
C2B	0.8052 (7)	−0.0666 (13)	−0.1822 (4)	0.0330 (18)
H2B	0.8273	−0.0415	−0.2141	0.040*
C3B	0.7786 (8)	−0.2282 (14)	−0.1709 (5)	0.044 (2)
H3B	0.7837	−0.3144	−0.1955	0.053*
C4B	0.7447 (7)	−0.2623 (13)	−0.1239 (4)	0.0319 (17)
H4B	0.7299	−0.3722	−0.1163	0.038*
C5B	0.7324 (6)	−0.1354 (10)	−0.0876 (4)	0.0234 (15)
H5B	0.7056	−0.1572	−0.0571	0.028*
C6B	0.7610 (5)	0.0242 (10)	−0.0979 (3)	0.0150 (11)
C7B	0.7587 (6)	0.1815 (10)	−0.0654 (3)	0.0193 (12)
N1C	0.8708 (5)	0.3277 (10)	0.1144 (3)	0.0250 (13)
N2C	1.0747 (5)	0.1100 (11)	0.3764 (3)	0.0290 (15)
C1C	0.8476 (6)	0.1934 (13)	0.1409 (4)	0.0285 (16)
H1C	0.7979	0.1333	0.1260	0.034*

C2C	0.8943 (6)	0.1394 (13)	0.1897 (4)	0.0273 (16)
H2C	0.8775	0.0429	0.2066	0.033*
C3C	0.9665 (6)	0.2319 (12)	0.2128 (4)	0.0258 (15)
C4C	0.9909 (6)	0.3704 (12)	0.1859 (4)	0.0245 (15)
H4C	1.0392	0.4349	0.2004	0.029*
C5C	0.9414 (6)	0.4112 (13)	0.1366 (4)	0.0278 (16)
H5C	0.9589	0.5034	0.1178	0.033*
C6C	1.0531 (6)	−0.0117 (14)	0.3392 (4)	0.0292 (17)
H6C	1.0603	−0.1232	0.3502	0.035*
C7C	1.0211 (6)	0.0213 (14)	0.2860 (4)	0.0305 (17)
H7C	1.0061	−0.0661	0.2616	0.037*
C8C	1.0115 (6)	0.1871 (13)	0.2690 (4)	0.0285 (16)
C9C	1.0388 (6)	0.3137 (13)	0.3059 (4)	0.0281 (17)
H9C	1.0366	0.4258	0.2952	0.034*
C10C	1.0697 (6)	0.2687 (13)	0.3594 (4)	0.0274 (16)
H10C	1.0876	0.3534	0.3844	0.033*
N1D	0.8591 (6)	0.6615 (10)	0.0215 (3)	0.0295 (13)
C1D	0.8627 (9)	0.8027 (14)	0.0499 (5)	0.052 (2)
H1D	0.8271	0.8120	0.0769	0.062*
C2D	0.9154 (9)	0.9350 (14)	0.0419 (6)	0.056 (2)
H2D	0.9132	1.0324	0.0623	0.067*
C3D	0.9708 (5)	0.9267 (9)	0.0047 (4)	0.0254 (15)
C4D	0.9664 (10)	0.7839 (17)	−0.0263 (6)	0.074 (3)
H4D	1.0018	0.7731	−0.0534	0.088*
C5D	0.9094 (9)	0.6560 (17)	−0.0174 (6)	0.061 (2)
H5D	0.9061	0.5618	−0.0397	0.073*

Atomic displacement parameters (Å²)

	U^{11}	U^{22}	U^{33}	U^{12}	U^{13}	U^{23}
Ag1	0.0296 (3)	0.0237 (3)	0.0211 (3)	0.0026 (3)	−0.0021 (2)	−0.0025 (3)
Ag2	0.0338 (3)	0.0364 (3)	0.0262 (3)	0.0085 (3)	−0.0050 (3)	−0.0129 (3)
S1A	0.0197 (9)	0.0220 (9)	0.0172 (6)	0.0037 (7)	−0.0003 (6)	−0.0005 (6)
S2A	0.0230 (10)	0.0312 (5)	0.0127 (7)	0.0039 (5)	−0.0013 (6)	−0.0048 (5)
N1A	0.0293 (9)	0.0175 (15)	0.0173 (6)	0.0017 (10)	−0.0019 (5)	0.0012 (7)
O1A	0.0198 (9)	0.038 (4)	0.032 (3)	0.0022 (8)	−0.0001 (7)	−0.003 (3)
O2A	0.035 (3)	0.026 (2)	0.0222 (19)	−0.001 (2)	0.006 (2)	−0.0004 (18)
C1A	0.012 (3)	0.0204 (10)	0.0124 (13)	0.0003 (13)	−0.0025 (14)	−0.0016 (7)
C2A	0.027 (4)	0.0326 (17)	0.0261 (17)	−0.005 (2)	0.004 (2)	−0.0145 (15)
C3A	0.026 (4)	0.0349 (19)	0.044 (3)	−0.004 (2)	0.012 (2)	−0.0069 (17)
C4A	0.036 (5)	0.033 (2)	0.044 (2)	0.001 (3)	0.009 (2)	−0.0090 (19)
C5A	0.025 (4)	0.0186 (14)	0.028 (2)	0.0043 (16)	0.005 (2)	0.0062 (12)
C6A	0.013 (3)	0.0137 (14)	0.0127 (12)	−0.0027 (12)	−0.0033 (13)	−0.0014 (8)
C7A	0.022 (2)	0.0131 (15)	0.0121 (8)	−0.0031 (12)	−0.0005 (12)	−0.0006 (7)
S1B	0.0460 (14)	0.0188 (9)	0.0377 (11)	−0.0079 (9)	0.0167 (10)	−0.0039 (7)
S2B	0.0234 (5)	0.0284 (4)	0.0224 (6)	0.0001 (3)	0.0050 (4)	−0.0062 (3)
N1B	0.030 (3)	0.0187 (15)	0.0322 (14)	0.0003 (15)	0.0071 (17)	0.0000 (10)
O1B	0.066 (4)	0.031 (3)	0.040 (2)	0.006 (3)	0.013 (2)	−0.004 (2)

O2B	0.0464 (14)	0.038 (4)	0.081 (6)	−0.0102 (10)	0.0187 (11)	−0.004 (4)
C1B	0.031 (3)	0.0179 (10)	0.0252 (18)	−0.0040 (12)	0.016 (2)	−0.0041 (8)
C2B	0.041 (5)	0.0277 (16)	0.033 (2)	0.001 (2)	0.014 (3)	−0.0123 (16)
C3B	0.059 (5)	0.0292 (18)	0.049 (3)	−0.003 (3)	0.024 (3)	−0.0114 (18)
C4B	0.032 (4)	0.0238 (19)	0.042 (3)	0.003 (2)	0.010 (3)	−0.0090 (19)
C5B	0.024 (4)	0.0146 (14)	0.034 (3)	−0.0018 (16)	0.013 (3)	−0.0010 (13)
C6B	0.013 (3)	0.0134 (14)	0.0197 (17)	0.0006 (14)	0.0063 (17)	−0.0022 (10)
C7B	0.021 (3)	0.0149 (15)	0.0217 (12)	0.0034 (15)	0.0038 (17)	−0.0039 (9)
N1C	0.0232 (16)	0.031 (2)	0.0206 (14)	0.0012 (15)	0.0020 (13)	0.0023 (15)
N2C	0.022 (4)	0.038 (2)	0.025 (2)	0.001 (2)	−0.004 (2)	0.0119 (15)
C1C	0.025 (3)	0.034 (2)	0.026 (2)	0.000 (2)	0.0010 (18)	0.0061 (18)
C2C	0.022 (2)	0.034 (3)	0.025 (2)	−0.001 (2)	0.0019 (19)	0.0066 (16)
C3C	0.021 (3)	0.033 (3)	0.0238 (18)	0.000 (2)	0.0028 (17)	0.0061 (15)
C4C	0.020 (3)	0.032 (3)	0.021 (2)	0.000 (2)	0.0021 (14)	0.0048 (19)
C5C	0.026 (2)	0.033 (3)	0.023 (2)	−0.001 (2)	−0.0012 (17)	0.0056 (18)
C6C	0.020 (4)	0.041 (2)	0.026 (2)	−0.003 (2)	0.001 (2)	0.0096 (14)
C7C	0.024 (4)	0.040 (2)	0.026 (2)	−0.004 (2)	0.000 (2)	0.0096 (14)
C8C	0.020 (3)	0.040 (2)	0.0249 (18)	−0.0031 (19)	0.0022 (18)	0.0093 (13)
C9C	0.022 (4)	0.037 (2)	0.0233 (19)	−0.001 (2)	−0.0014 (19)	0.0116 (15)
C10C	0.020 (4)	0.038 (2)	0.023 (2)	0.002 (2)	0.000 (2)	0.0114 (16)
N1D	0.034 (2)	0.0230 (12)	0.032 (3)	0.0021 (15)	0.007 (2)	−0.0055 (14)
C1D	0.084 (5)	0.0292 (17)	0.053 (4)	−0.021 (2)	0.048 (4)	−0.017 (2)
C2D	0.083 (4)	0.026 (2)	0.072 (4)	−0.018 (3)	0.055 (3)	−0.017 (3)
C3D	0.029 (3)	0.024 (3)	0.023 (3)	0.001 (2)	0.004 (2)	0.000 (2)
C4D	0.088 (5)	0.054 (3)	0.094 (5)	−0.038 (3)	0.064 (4)	−0.046 (3)
C5D	0.075 (4)	0.054 (4)	0.063 (3)	−0.034 (3)	0.042 (3)	−0.037 (3)

Geometric parameters (Å, º)

Ag1—N1D	2.312 (8)	C4B—C5B	1.387 (12)
Ag1—N1C	2.373 (7)	C4B—H4B	0.9300
Ag1—S2B	2.492 (2)	C5B—C6B	1.380 (11)
Ag1—N1A	2.502 (8)	C5B—H5B	0.9300
Ag1—Ag2	2.8859 (10)	C6B—C7B	1.493 (11)
Ag2—N2C^{i}	2.349 (8)	N1C—C5C	1.320 (12)
Ag2—S2A	2.448 (2)	N1C—C1C	1.332 (12)
Ag2—S2B	2.566 (2)	N2C—C10C	1.330 (12)
S1A—O1A	1.430 (7)	N2C—C6C	1.346 (13)
S1A—O2A	1.434 (6)	C1C—C2C	1.385 (12)
S1A—N1A	1.652 (7)	C1C—H1C	0.9300
S1A—C1A	1.749 (8)	C2C—C3C	1.383 (13)
S2A—C7A	1.708 (8)	C2C—H2C	0.9300
N1A—C7A	1.311 (10)	C3C—C4C	1.371 (12)
C1A—C2A	1.376 (11)	C3C—C8C	1.508 (10)
C1A—C6A	1.389 (10)	C4C—C5C	1.385 (12)
C2A—C3A	1.395 (14)	C4C—H4C	0.9300
C2A—H2A	0.9300	C5C—H5C	0.9300
C3A—C4A	1.368 (15)	C6C—C7C	1.370 (13)

C3A—H3A	0.9300	C6C—H6C	0.9300
C4A—C5A	1.405 (13)	C7C—C8C	1.386 (14)
C4A—H4A	0.9300	C7C—H7C	0.9300
C5A—C6A	1.383 (11)	C8C—C9C	1.387 (14)
C5A—H5A	0.9300	C9C—C10C	1.394 (12)
C6A—C7A	1.494 (11)	C9C—H9C	0.9300
S1B—O2B	1.423 (9)	C10C—H10C	0.9300
S1B—O1B	1.427 (8)	N1D—C1D	1.324 (12)
S1B—N1B	1.659 (8)	N1D—C5D	1.325 (14)
S1B—C1B	1.788 (9)	C1D—C2D	1.361 (15)
S2B—C7B	1.730 (9)	C1D—H1D	0.9300
N1B—C7B	1.289 (11)	C2D—C3D	1.347 (13)
C1B—C2B	1.351 (12)	C2D—H2D	0.9300
C1B—C6B	1.375 (11)	C3D—C4D	1.370 (14)
C2B—C3B	1.391 (15)	C3D—C3D^{ii}	1.510 (11)
C2B—H2B	0.9300	C4D—C5D	1.382 (16)
C3B—C4B	1.376 (15)	C4D—H4D	0.9300
C3B—H3B	0.9300	C5D—H5D	0.9300
Ag2···S2A^{iii}	3.046 (2)		
N1D—Ag1—N1C	97.0 (3)	C2B—C3B—H3B	119.5
N1D—Ag1—S2B	137.1 (2)	C3B—C4B—C5B	121.1 (10)
N1C—Ag1—S2B	103.3 (2)	C3B—C4B—H4B	119.4
N1D—Ag1—N1A	96.3 (3)	C5B—C4B—H4B	119.4
N1C—Ag1—N1A	96.7 (2)	C6B—C5B—C4B	118.0 (8)
S2B—Ag1—N1A	117.91 (18)	C6B—C5B—H5B	121.0
N1D—Ag1—Ag2	112.3 (2)	C4B—C5B—H5B	121.0
N1C—Ag1—Ag2	150.65 (19)	C1B—C6B—C5B	119.0 (8)
S2B—Ag1—Ag2	56.43 (6)	C1B—C6B—C7B	111.5 (7)
N1A—Ag1—Ag2	78.43 (17)	C5B—C6B—C7B	129.5 (7)
N2C^{i}—Ag2—S2A	118.3 (2)	N1B—C7B—C6B	115.8 (7)
N2C^{i}—Ag2—S2B	97.0 (2)	N1B—C7B—S2B	124.3 (7)
S2A—Ag2—S2B	141.04 (8)	C6B—C7B—S2B	119.9 (6)
N2C^{i}—Ag2—Ag1	128.9 (2)	C5C—N1C—C1C	117.4 (8)
S2A—Ag2—Ag1	89.13 (6)	C5C—N1C—Ag1	121.9 (6)
S2B—Ag2—Ag1	54.01 (5)	C1C—N1C—Ag1	119.7 (6)
O1A—S1A—O2A	116.5 (4)	C10C—N2C—C6C	118.0 (8)
O1A—S1A—N1A	110.8 (4)	N1C—C1C—C2C	122.8 (9)
O2A—S1A—N1A	109.0 (4)	N1C—C1C—H1C	118.6
O1A—S1A—C1A	109.6 (4)	C2C—C1C—H1C	118.6
O2A—S1A—C1A	112.9 (4)	C3C—C2C—C1C	118.7 (9)
N1A—S1A—C1A	96.2 (4)	C3C—C2C—H2C	120.7
C7A—S2A—Ag2	106.5 (3)	C1C—C2C—H2C	120.7
C7A—N1A—S1A	110.8 (6)	C4C—C3C—C2C	119.0 (8)
C7A—N1A—Ag1	117.7 (5)	C4C—C3C—C8C	121.5 (8)
S1A—N1A—Ag1	121.3 (4)	C2C—C3C—C8C	119.4 (8)
C2A—C1A—C6A	122.4 (8)	C3C—C4C—C5C	117.9 (9)

C2A—C1A—S1A	129.9 (7)	C3C—C4C—H4C	121.0
C6A—C1A—S1A	107.7 (6)	C5C—C4C—H4C	121.0
C1A—C2A—C3A	117.8 (9)	N1C—C5C—C4C	124.2 (9)
C1A—C2A—H2A	121.1	N1C—C5C—H5C	117.9
C3A—C2A—H2A	121.1	C4C—C5C—H5C	117.9
C4A—C3A—C2A	119.8 (10)	N2C—C6C—C7C	122.9 (10)
C4A—C3A—H3A	120.1	N2C—C6C—H6C	118.5
C2A—C3A—H3A	120.1	C7C—C6C—H6C	118.5
C3A—C4A—C5A	122.9 (10)	C6C—C7C—C8C	119.0 (10)
C3A—C4A—H4A	118.5	C6C—C7C—H7C	120.5
C5A—C4A—H4A	118.5	C8C—C7C—H7C	120.5
C6A—C5A—C4A	116.8 (9)	C7C—C8C—C9C	118.7 (8)
C6A—C5A—H5A	121.6	C7C—C8C—C3C	121.4 (9)
C4A—C5A—H5A	121.6	C9C—C8C—C3C	119.7 (9)
C5A—C6A—C1A	120.2 (8)	C8C—C9C—C10C	118.3 (9)
C5A—C6A—C7A	129.6 (7)	C8C—C9C—H9C	120.8
C1A—C6A—C7A	110.0 (7)	C10C—C9C—H9C	120.8
N1A—C7A—C6A	115.2 (7)	N2C—C10C—C9C	122.8 (10)
N1A—C7A—S2A	125.8 (6)	N2C—C10C—H10C	118.6
C6A—C7A—S2A	119.1 (6)	C9C—C10C—H10C	118.6
O2B—S1B—O1B	117.5 (5)	C1D—N1D—C5D	115.8 (9)
O2B—S1B—N1B	109.3 (5)	C1D—N1D—Ag1	121.7 (7)
O1B—S1B—N1B	109.8 (5)	C5D—N1D—Ag1	122.5 (7)
O2B—S1B—C1B	111.2 (5)	N1D—C1D—C2D	123.8 (10)
O1B—S1B—C1B	111.0 (5)	N1D—C1D—H1D	118.1
N1B—S1B—C1B	95.9 (4)	C2D—C1D—H1D	118.1
C7B—S2B—Ag1	101.8 (3)	C3D—C2D—C1D	120.9 (10)
C7B—S2B—Ag2	99.4 (3)	C3D—C2D—H2D	119.6
Ag1—S2B—Ag2	69.56 (7)	C1D—C2D—H2D	119.6
C7B—N1B—S1B	110.9 (6)	C2D—C3D—C4D	116.4 (8)
C2B—C1B—C6B	124.3 (9)	C2D—C3D—C3D^{ii}	121.2 (10)
C2B—C1B—S1B	129.7 (7)	C4D—C3D—C3D^{ii}	122.2 (11)
C6B—C1B—S1B	106.0 (6)	C3D—C4D—C5D	120.0 (11)
C1B—C2B—C3B	116.4 (10)	C3D—C4D—H4D	120.0
C1B—C2B—H2B	121.8	C5D—C4D—H4D	120.0
C3B—C2B—H2B	121.8	N1D—C5D—C4D	123.0 (11)
C4B—C3B—C2B	120.9 (10)	N1D—C5D—H5D	118.5
C4B—C3B—H3B	119.5	C4D—C5D—H5D	118.5

Symmetry codes: (i) $x-1/2, -y+1/2, z-1/2$; (ii) $-x+2, -y+2, -z$; (iii) $-x+1, -y+1, -z$.